Inorganic Chemistry

Article

pubs.acs.org/IC

Cationic Copper(II)-containing Surfactants: Molecular Structures, Film Morphology, and Influence on the Alignment of Nematic Mesogens

Cláudio N. Verani,*[,†] Jeffery Driscoll,[†] Paul H. Keyes,[‡] and Mary Jane Heeg[†]

[†]Department of Chemistry and [‡]Department of Physics and Astronomy, Wayne State University, 5101 Cass Avenue, Room 161, Detroit, Michigan 48202, United States

Supporting Information

ABSTRACT: We discuss the synthesis and amphiphilic behavior of the cationic metallosurfactants $[(L^{Py14})_2Cu^{II}ClO_4]ClO_4$ (**1**), $[(L^{Py16})_2Cu^{II}ClO_4]ClO_4$ (**2**), $[(L^{Py18})_2Cu^{II}ClO_4]ClO_4$ (**3**), $[(L^{Py18})_2Cu^{II}NO_3]NO_3$ (**4**), $[(L^{Py18})_2Cu^{II}Cl]Cl$ (**5**), and $[(L^{Py18})_2Cu^{II}Br]Br$ (**6**) obtained by treatment of the appropriate alkylaminemethyl-2-pyridine ligand containing tetra-, hexa-, or octadecyl chains with copper salts. These metallosurfactants show excellent agreement between infrared spectroscopic bands, spectrometric masses with isotopic patterns, and elemental composition. Single-crystal X-ray data available for **1**, **2**, **5** and the previously published **3** reveal a trigonal bipyramidal copper(II) ion bound at the basal plane to the amine and pyridine of each alkylaminemethylpyridine ligand and an anionic coligand to the apical position. Except for the surfactant with the shortest tetradecyl (C_{14}) chain, these species yield Langmuir films with collapse pressures of 45−55 mN·m^{-1} and average areas of ca. 50 Å^2. A plateau around 15 mN·m^{-1} is observed for **3**, **4**, and **5** and associated with the formation of dendritic domains about 50 μm in size. Species **2** and **6** lack this plateau and show domains of ca. 5 μm. Once transferred onto solid substrates, the resulting Langmuir−Blodgett film of **3** at 18 mN·m^{-1} influences the alignment of the nematic liquid crystal *N*-(4-methoxybenzylidene)-4-butylaniline.

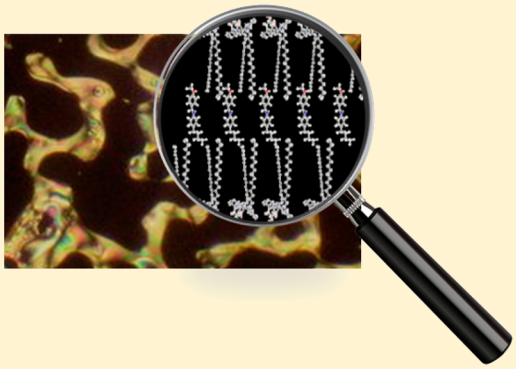

INTRODUCTION

Metallopolymers,[1] metallomesogens,[2,3] and metallosurfactants[4−6] are promising as materials for high-end applications in molecular electronics and display technology,[7,8] analyte sensing,[9,10] catalysis,[11] and photophysics.[12] These materials combine the traditional behavior of organic materials with the versatility of transition metals to generate supramolecular topologies.[13,14] Because of this relevance, our group is engaged in the development of new metallosurfactants with unique electronic and interfacial properties. We have focused on the strengths and limitations of amphiphilic species containing first-row transition metal ions,[15−18] while emphasizing the use of multidentate ligands to prevent dissociation at the air/water interface. In this regard, incorporation of copper is particularly relevant due to its abundance, affordability, and rich chemistry associated with multiple geometries, coordination numbers, and redox states. We have observed (i) the viability of exhaustive redox cycling on Cu(II)/salycilaldimine surfactants,[19] (ii) the Langmuir−Blodgett (LB) film patterning in magnetic carboxylate-supported [μ-oxo-Cu_4] clusters,[20] and (iii) the effect of subphase changes in LB monolayers with [Cu_2] and [Cu_4] surfactants.[21] Particularly relevant to this study, we also evaluated a series of single-tail copper(II)-containing surfactants with aminomethylpyridine headgroups, $[L^{Py_n}Cu^{II}X_2]$ with n = C_{10}, C_{14}, C_{16}, C_{18} and X = Cl^- and Br^-, demonstrating the formation of biphasic patterned Langmuir films at the air/water interface.[22] The intricate film topology seems associated with changes on the length of the alkyl chains and on the nature of the apical halogen coligand. Comparative molecular organization of LB monolayers of the unmetallated ligand L^{Py18}, the single-tail $[L^{Py18}Cu^{II}Cl_2]$, and the double-tail $[(L^{Py18})_2Cu^{II}Cl]Cl$ complexes was studied by means of surface-selective vibrational sum frequency generation spectroscopy[23] and demonstrates that copper(II) coordination enhances the molecular alignment and reduces the fraction of gauche defects of the alkyl chains. Monolayers of the double-tail surfactant show lower degree of packing and conformational order than that observed for the single-tail counterpart, likely because of the presence of a bulkier headgroup. Remarkably, these $[(L^{Py18})_2Cu^{II}X]^+$ species also display tunable thermotropic mesomorphism[24] associated with the nature of the apical coligand: the bromido species $[(L^{Py18})_2Cu^{II}Br]^+$ shows a clear smectic A phase at 110 °C, while the nitro and perchloro species $[(L^{Py18})_2Cu^{II}NO_3]^+$ and $[(L^{Py18})_2Cu^{II}ClO_4]^+$ show increasingly higher temperatures of 136 and 153 °C, respectively. The behavior of these complexes suggests that at low temperatures the crystalline materials are bilayered structures with interdigitated alkyl tails, while at higher temperatures the tails undergo rapid conformational changes that force these layers to swell until the opposing alkyl

Received: February 19, 2014
Published: May 9, 2014

   dx.doi.org/10.1021/ic5004098 | *Inorg. Chem.* 2014, 53, 5647−5655

chains are separated from each other, and the mesophase is a monolayer smectic A.

In this Article we expand on the family of available copper-containing surfactants and hypothesize that the LB films of these species may be able to influence the orientation of nematic liquid crystals. This is a relevant first step toward the development of redox-responsive liquid-crystal displays. We present a detailed study of the synthesis, isolation, and characterization of a new series of copper surfactants, namely, $[(L^{Py14})_2Cu^{II}ClO_4]ClO_4$ (**1**), $[(L^{Py16})_2Cu^{II}ClO_4]ClO_4$ (**2**), $[(L^{Py18})_2Cu^{II}ClO_4]ClO_4$ (**3**), $[(L^{Py18})_2Cu^{II}NO_3]NO_3$ (**4**), $[(L^{Py18})_2Cu^{II}Cl]Cl$ (**5**), and $[(L^{Py18})_2Cu^{II}Br]Br$ (**6**), as shown in Scheme 1. We examine their interfacial behavior, domain

Scheme 1

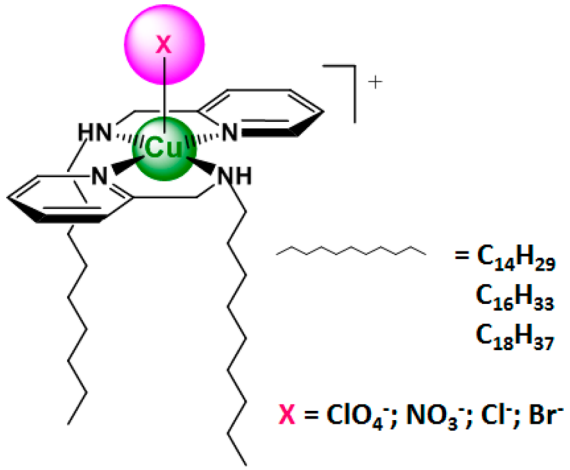

$[(L^{Py14})_2Cu^{II}ClO_4]ClO_4$ (**1**)

$[(L^{Py16})_2Cu^{II}ClO_4]ClO_4$ (**2**)

$[(L^{Py18})_2Cu^{II}ClO_4]ClO_4$ (**3**)

$[(L^{Py18})_2Cu^{II}NO_3]NO_3$ (**4**)

$[(L^{Py18})_2Cu^{II}Cl]Cl$ (**5**)

$[(L^{Py18})_2Cu^{II}Br]Br$ (**6**)

evolution and patterning at the air−water interface, and morphology of the resulting LB films. Finally, considering the increasing experimental[25−31] and theoretical[32,33] interest in the influence of modified surfaces as orientation directors for liquid crystals, we demonstrate that interfacial contact between the LB film of a select metallosurfactant and *N*-(4-methoxybenzylidene)-4-butylaniline (MBBA) leads to alterations of alignment, as monitored by optical microscopy.

EXPERIMENTAL SECTION

Materials and Methods. Starting materials were purchased from commercial sources. Dichloromethane was purified using an I.T. solvent purification system. Infrared (IR) spectra were measured from 4000 to 400 cm^{-1} using KBr pellets on a Tensor 27 FTIR-spectrophotometer. Electrospray ionization (ESI) mass spectra in the positive mode were measured on a Micromass QuattroLC triple quadrupole mass spectrometer with an electrospray/APCI source and Walters Alliance 2695 LC, autosampler, and photodiode array UV detector. Experimental assignments were simulated based on peak position and isotopic distributions. Elemental analyses were performed by Midwest Microlab, Indianapolis, Indiana. UV−visible spectra were collected in 1.0×10^{-3} M dichloromethane using a Varian Cary 50 spectrophotometer in the range of 200 to 1100 nm.

Syntheses. The ligands L^{Py_n}, (n = C_{14}, C_{16}, and C_{18}) were obtained as previously described in the literature.[22]

Caution! *Complexes* ***1−3*** *are perchlorate salts and therefore are potentially explosive. Although no problems were observed in this study, small amounts of material should be used for synthesis and analyses, and proper safety precautions should be taken.*

Complexes **1−6** were synthesized in MeOH by treatment of the appropriate ligand with different copper salts in a 2:1 ligand-to-metal ratio.[24] The complexes were isolated as solids and recrystallized in specific solvent mixtures. Analytical details follow.

*$[(L^{Py14})_2Cu^{II}ClO_4]ClO_4$ (**1**).* Prepared by treatment of L^{Py14} with $Cu(ClO_4)_2 \cdot 6H_2O$. A royal blue solution yielded violet X-ray quality crystals from a 1:1 isopropanol−chloroform solvent combination. Yield = 88%. Elemental analysis calculated for $C_{40}H_{72}Cl_2CuN_4O_8$ (MW = 871.48 g/mol): C, 55.13; H, 8.33; N, 6.43%. Found: C, 55.29; H, 8.28; N 6.49%. IR (KBr, cm^{-1}) 2917(s) 2850(s) (alkyl- CH−); 1486(m) (CH_2CH_2); 1613(s) 1574(m) 1486(m) ($C{=}N_{pyr}$) and (R′−NH−R); 1108(m) 1060(m) 1044(m) 624(s) (ClO_4^-); ESI Pos. in MeOH: m/z (100%) = 768.44 for $[(L^{Py14})_2Cu^{II}ClO_4]^+$. UV−visible ($CH_2Cl_2$, 1.0×10^{-4} M, nm, ($M^{-1}\cdot cm^{-1}$)) 260 (13 000); 300(sh) (∼3000); 610 (125). melting point (mp) = 163−165 °C.

*$[(L^{Py16})_2Cu^{II}ClO_4]ClO_4$ (**2**).* Prepared by treatment of L^{Py16} with $Cu(ClO_4)_2 \cdot 6H_2O$. A royal blue solution yielded violet X-ray quality crystals from a 1:1 ethanol−chloroform solvent combination. Yield = 82%. Elemental analysis calculated for $C_{44}H_{80}Cl_2CuN_4O_8$ (MW = 927.59 g/mol): C, 56.97; H, 8.69; N, 6.04%. Found: C, 56.78; H, 8.48; N 6.08%. IR (KBr, cm^{-1}) 2918(s) 2849(s) (alkyl- CH−); 1486(m) (CH_2CH_2); 1610(s) 1572(m) 1486(m) ($C{=}N_{pyr}$) and (C=C); 1575(s) (R′−NH−R); 1110(m) 1065(m) 1045(m) 625(s) (ClO_4^-); ESI Pos. in MeOH: m/z (100%) = 826.62 for $[(L^{Py16})_2Cu^{II}ClO_4]^+$. UV−visible ($CH_2Cl_2$, 1.0×10^{-4} M, nm ($M^{-1}\cdot cm^{-1}$)) 260 (13 500); 300(sh) (∼3,000); 610 (120). mp = 160−163 °C.

*$[(L^{Py18})_2Cu^{II}ClO_4]ClO_4$ (**3**).* Prepared by treatment of L^{Py18} with $Cu(ClO_4)_2 \cdot 6H_2O$. A royal blue solution yielded violet X-ray quality crystals from a 1:1 methanol−chloroform solvent combination. Yield = 87%. Elemental analysis calculated for $C_{48}H_{88}Cl_2CuN_4O_8$ (MW = 983.69 g/mol): C, 58.61; H, 9.02; N, 5.70%. Found: C, 58.31; H, 8.82; N 5.70%. IR (KBr, cm^{-1}) 2919(s) 2850(s) (alkyl- CH−); 1486(m) (CH_2CH_2); 1613(s) 1574(m) 1486(m) ($C{=}N_{pyr}$) and (C=C); 1574(s) (R′−NH−R); 1108(m) 1063(m) 1043(m) 624(s) (ClO_4^-); ESI Pos. in MeOH: m/z (100%) = 882.58 for $[(L^{Py18})_2Cu^{II}ClO_4]^+$. UV−visible ($CH_2Cl_2$, 1.0×10^{-4} M, nm ($M^{-1}\cdot cm^{-1}$)) 260 (15 000); 300(sh) (∼3000); 610 (125). mp = 152−154 °C.

*$[(L^{Py18})_2Cu^{II}NO_3]NO_3$ (**4**).* Prepared via treatment of L^{Py18} with $Cu(NO_3)_2 \cdot 2.5H_2O$, giving a violet powder. Yield = 84%. Elemental analysis calculated for $C_{48}H_{90}CuN_6O_6$ (MW = 908.81 g/mol): C, 63.44; H, 9.76; N, 9.25%. Found: C, 63.91; H, 9.48; N 9.15%. IR (KBr, cm^{-1}) (R′−NH−R); 2847(s), 2914(s) (alkyl- CH−); 1430(m) (CH_2CH_2); 1609(s) 1476(m) ($C{=}N_{pyr}$) and (C=C); 1405(s) 1340(s) 1305(s) (NO_3^-); ESI Pos. in MeOH: m/z (100%) = 845.6 for $[(L^{Py18})_2Cu^{II}NO_3]^+$. UV−visible ($CH_2Cl_2$, 1.0×10^{-4} M, nm ($M^{-1}\cdot cm^{-1}$)) 260 (12 900); 300(sh) (∼3000); 690 (120). mp = 152−154 °C.

*$[(L^{Py18})_2Cu^{II}Cl]Cl.2CH_3CN$ (**5**).* Prepared by treatment of L^{Py18} with $CuCl_2 \cdot 2H_2O$. Dark blue X-ray quality crystals were isolated from an isopropanol−acetonitrile solvent combination. Yield = 84%. Elemental analysis calculated for $C_{52}H_{94}Br_2Cu_1N_6$ (MW = 937.61 g/mol): C, 66.60; H, 10.10; N, 8.96%. Found: C, 66.90; H, 10.29; N, 8.52%. IR (KBr, cm^{-1}) 2916(s), 2849(s) (alkyl- CH−); 1376 ($C{=}N_{aromatic}$); 1607(s) 1571(m) 1471(s); ($C{=}N_{pyr}$) and (C=C); ESI Pos. in MeOH: m/z (100%) = 818.6 for $[(L^{Py18})_2Cu^{II}Cl]^+$. UV−visible ($CH_2Cl_2$, 1.0×10^{-4} M, nm ($M^{-1}\cdot cm^{-1}$)) 260 (13 000); 290 (∼4500); 710 (340). mp = 115−116 °C. The compound is noted as $[(L^{Py18})_2Cu^{II}Cl]Cl$ (**5**) throughout the text.

*$[(L^{Py18})_2Cu^{II}Br]Br$ (**6**).* Prepared by treating L^{Py18} with $CuBr_2$, yielding a violet powder. Yield = 84%. Elemental analysis calculated for $C_{48}H_{88}Br_2Cu_1N_4$ (MW = 944.61 g/mol): C, 61.03; H, 9.39; N, 5.93%. Found: C, 60.31; H, 8.70; N 5.91%. IR (KBr, cm^{-1}) 2849(s), 2918(s)

dx.doi.org/10.1021/ic5004098 | *Inorg. Chem.* 2014, 53, 5647−5655

Table 1. Crystallographic Data for 1, 2, and 5

complex	1	2	5
formula	$C_{40}H_{72}Cl_2CuN_4O_8$	$C_{44}H_{80}Cl_2CuN_4O_8$	$C_{52}H_{94}Cl_2CuN_6$
fw	871.46	927.56	937.77
space group	triclinic, $P\bar{1}$	triclinic, $P\bar{1}$	triclinic, $P\bar{1}$
a (Å)	9.9429(2)	9.9466(3)	8.9223(3)
b (Å)	11.8010(3)	11.7956(4)	10.9905(4)
c (Å)	21.0849(5)	22.4258(9)	29.0501(10)
α (deg)	80.5890(10)	85.784(3)	89.104(2)
β (deg)	78.0980(10)	79.337 (3)	82.929(2)
γ (deg)	69.2970(10)	69.310(2)	73.348(2)
V (Å^3)	2253.39(9)	2418.84(15)	2707.87(16)
Z	2	2	2
temp (K)	100(2)	100(2)	100(2)
λ (Å)	0.710 73	0.710 73	0.710 73
density, cal (g cm^{-3})	1.284	1.274	1.150
μ (mm^{-1})	0.655	0.614	0.540
$R(F)$ (%)[a]	3.81	7.68	4.72
$Rw(F)$ (%)[a]	8.53	19.67	10.41

[a] $R(F) = \sum||Fo| - |Fc||/\sum|Fo|$; $Rw(F) = [\sum w(Fo^2 - Fc^2)^2/\sum w(Fo^2)^2]^{1/2}$ for $I > 2\sigma(I)$.

(alkyl- CH−); 1364 (C═$N_{aromatic}$); 1148(s) (R′−NH−R); 1609(s) 1570(m) 1468(m) (C═N_{pyr}) and (C═C); ESI Pos. in MeOH: m/z (100%) = 862.5 for $[(L^{Py18})_2Cu^{II}Br]^+$. UV−visible ($CH_2Cl_2$, 1.0 × 10^{-4} M, nm (M^{-1}·cm^{-1})) 260 (12 900); 290 (∼4800); 790 (325). mp = 134−135 °C.

X-ray Structural Determination for 1, 2, and 5. Diffraction data were measured on a Bruker *APEX-II* κ-geometry diffractometer with Mo radiation and graphite monochromator at 100 K. Frames were collected with the detector at 40 mm, 0.3° between each frame, and 10−20 s/frame. All frame data were indexed and integrated with the manufacturer's *SMART*, *SAINT*, and *SADABS* software.[34] All structures were refined using the *SHELX-97* software.[35] A summary of the crystal structure parameters is contained in Table 1. Compound **1** ($C_{40}H_{72}Cl_2CuN_4O_8$, CCDC # 933201) crystallized as violet plates. A total of 50 016 data points were measured, yielding 12 750 unique averaged *hkl* data. The asymmetric unit contains one $[(L^{Py14})_2Cu^{II}ClO_4]^+$ cation electrostatically associated with a perchlorate anion. Compound **2** ($C_{44}H_{80}Cl_2CuN_4O_8$, CCDC # 933202) crystallized as violet plates. A total of 35 477 reflections were counted, producing 12 035 unique averaged data. Similar to **1**, the asymmetric unit contains one $[(L^{Py16})_2Cu^{II}ClO_4]^+$ associated with one perchlorate counterion. The very disordered pendant chains were described in partial occupancy positions and held isotropic during refinement. Both species **1** and **2** have hydrogen atoms placed in calculated positions, and both ammine hydrogen atoms were involved in hydrogen bonding with perchlorato oxygen atoms. Compound **5** ($C_{52}H_{94}N_6Cl_2Cu_1$, CCDC # 933203) formed thin blue rods. A total of 47 079 reflections were harvested from 3174 frames, merging into 13 279 unique reflections. Hydrogen atoms were calculated or observed. The two long terminal chains of each ligand are unusually ordered for this type of complex. Both amine hydrogen atoms associate with Cl$^-$ through hydrogen bonds. The asymmetric unit contains one $[(L^{Py18})_2Cu^{II}Cl]^+$ cation electrostatically associated with a Cl$^-$ counterion and two acetonitrile solvates.

Isothermal Compression and Langmuir−Blodgett Deposition. Measurement of the surface pressure versus area (π vs A) isotherms was carried out on a KSV minitrough equipped with computer-controlled moveable barriers. Symmetric compression of the monolayer utilized two interlinked leakproof hydrophilic Delrin surface barriers with a form-sintered single piece, nonporous polytetrafluoroethylene trough with a surface area of 273 cm^2. The subphase temperature (22.8 ± 0.5 °C) was controlled via a metal heating/cooling base plate operated by a water recirculating Julabo water bath. Ultrapure water (Barnstead NANOpure) with a resistivity of 17.5−18 MΩ·cm^{-1} was used in all experiments. Impurities present at the surface of the freshly poured aqueous subphase were removed by vacuum after the compression of the barriers. Spreading solutions were prepared in spectroscopy-grade chloroform. A known quantity (typically 25 μL) of freshly prepared surfactant solution with a known concentration of 1 mg·mL^{-1} was then spread on the clean aqueous subphase. The system was allowed to equilibrate for approximately 10 min before monolayer compression. The π versus A isotherms were obtained at compression rates of 5−10 mm·min^{-1}. A 40 × 40 mm paper plate was suspended from a film balance interfaced with a digital display and a computer to measure the pressure.[36] At least three independent measurements were carried out per sample, with excellent reproducibility attained. Films were transferred to precleaned glass microslides (Gold Seal, 24.99 × 50.0 × 1.07 mm) dipped into the subphase prior to the addition of the surfactant. Lateral compression was begun at 4.0 mm·min^{-1}, while the barrier speed was decreased stepwise to 1.0 mm·min^{-1} prior to reaching the targeted pressure to allow for a very stable film at 18 mN·m^{-1}. The resulting film was allowed to stand for 10 min with no barrier movement allowing for homogeneous deposition. Several slides were prepared at this deposition pressure.

Brewster Angle Microscopy. A KSV-Optrel BAM 300 with a HeNe laser (10 mW, 632.8 nm) and a CCD detector was used in all micrographs. A compression rate of 5 mm/min was chosen to maintain a homogeneous film growth on the monolayer. The field of view was 800 × 600 μm, and the lateral resolution was about 1−2 μm.

Polarized Optical Microscopy. Observations of the behavior of MBBA were performed on the stage of a Nikon Labphot polarizing microscope using a 40× objective. The sample temperatures were varied using a Mettler FP82 hot-stage controlled by a Mettler FP80 central processor. Images were collected using a Canon SD-760 digital camera mounted on the microscope. Samples of MBBA were placed in between glass slides and sandwiched under different conditions: (a) under untreated slides, (b) two slides coated with a randomly oriented film resulting from solvent evaporation, (c) with one singly coated slide and one untreated slide, and (d) with both slides coated with films of **3** at 18 mN·m^{-1}. The slides were inserted into the microscope, heated above their isotropic temperature, and then allowed to cool to room temperature. Experiments were repeated in triplicates, and images were taken to catalogue the progress.

RESULTS AND DISCUSSION

Synthesis and Characterization. Amphiphilic ligands were synthesized by the addition of 2-pyridinecarboxyaldehyde to 1-decylamine, 1-hexadecylamine, or 1-octadecylamine, followed by reduction with sodium borohydride in methanol. Complexes **1**−**6** were synthesized by treating the appropriate

dx.doi.org/10.1021/ic5004098 | Inorg. Chem. 2014, 53, 5647−5655

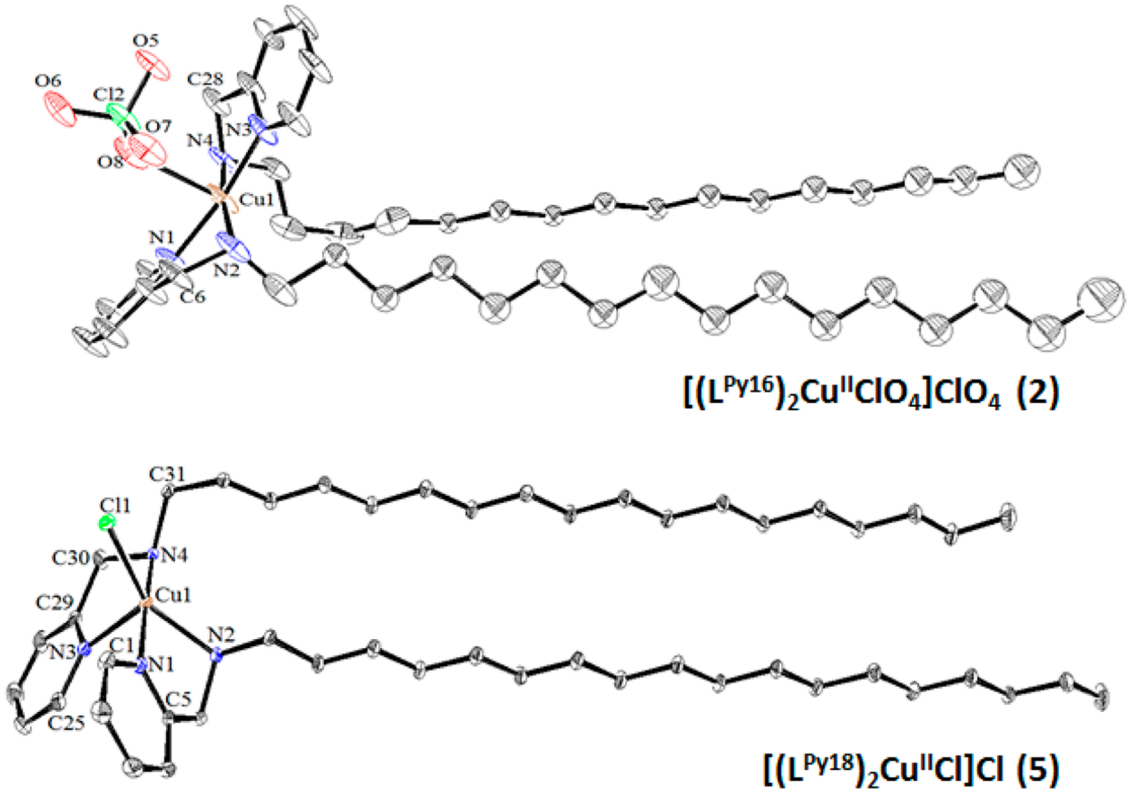

Figure 1. ORTEP diagrams for **2** and **5** at the 40% probability level and selected bond lengths (Å) and angles (deg). For **2**: Cu(1)−N(1) = 2.007(3), Cu(1)−N(2) = 2.017(3), Cu(1)−N(3) = 2.000(3), Cu(1)−N(4) = 2.013(3); C−$C_{ring\ average}$ = 1.383 Å, C−$C_{alkyl\ average}$= 1.539 Å; N(3)−Cu(1)−N(1) = 171.59(17), N(3)−Cu(1)−(N4) = 81.41(13), N(2)−Cu(1)−(N4) = 169.64(18), N(3)−Cu(1)−(N1) = 171.59(17), N(3)−Cu(1)−(N2) = 100.02(14), N(1)−Cu(1)−N(2) = 81.21(13), N(1)−Cu(1)−N(4) = 98.88(4)°. For **5**: Cu(1)−N(1) = 2.0108(17), Cu(1)−N(2) = 2.1038(16), Cu(1)−N(3) = 2.1560(17), Cu(1)−N(4) = 2.0433(16); C−$C_{ring\ average}$ = 1.377 Å, C−$C_{alkyl\ average}$= 1.521 Å; N(4)−Cu(1)−N(2) = 94.12(6), N(3)−Cu(1)−(N4) = 81.34(6), N(3)−Cu(1)−(N1) = 92.67(67), N(3)−Cu(1)−(N2) = 102.64(6), N(1)−Cu(1)−N(2) = 80.36(6), N(1)−Cu(1)−N(4) = 170.84(7), N(1)−Cu(1)−Cl(1) = 95.10(5), N(4)−Cu(1)−Cl(1) = 93.48(5), N(2)−Cu(1)−Cl(1) = 146.90(5)°.

ligand with copper(II) perchlorate (**1**−**3**), nitrate (**4**), chloride (**5**), and bromide (**6**) salts and isolated as microcrystalline powders or crystals. All complexes were thoroughly characterized using ESI^+ mass spectrometry, IR and UV−visible spectroscopy, elemental analyses, and melting points. Although the bands associated with the copper-halogen bonds are outside of the detection range of the instrument, successful identification of perchlorates and nitrates indicated the presence of coordinated and uncoordinated anionic species.[37] The IR bands arising from the metal-bound perchloro coligand appear at 1108 cm^{-1}, 1063 cm^{-1}, and 624 cm^{-1}. An additional band at 1043 cm^{-1} and typical of free perchlorate counterions is also observed. The free nitrate ions appear at 1411 and 1331 cm^{-1}, whereas the coordinated nitrato coligand was detected at 1308 cm^{-1}. Other bands associated with the ligands displayed minor shifts, suggesting that the electronic density of the bonds have been altered upon coordination.[38] The ESI^+ mass analysis of **1**−**6** in methanol shows peak clusters with m/z = 768.4 for **1**, 826.6 for **2**, 882.6 for **3**, 845.6 for **4**, 818.6 for **5**, and 862.5 for **6**, corresponding to the fragment $[(L^{Py_n})_2Cu^{II}X]^+$. Each complex displayed unique fragment profiles associated with the expected isotopic distributions. Complexes **1**−**3** and **5** show similar fragment patterns due to the presence of chloride atoms, while **4** and **6** show patterns associated with their respective anionic ligands, that is, nitrato and bromo, (Supporting Information, Figure S1). The UV−visible spectra of **1**−**6** taken as 1.0×10^{-3} M dichloromethane solutions reveal intense $\sigma \rightarrow \pi^*$ and/or $\pi \rightarrow \pi^*$ intraligand bands at 260 nm ($\varepsilon \approx 15$ 000 $M^{-1}\cdot cm^{-1}$) along with an ill-defined shoulder band at ∼300 nm attributed to pyridine-to-copper(II) charge transfer, and faint d−d transitions around 610 and 790 nm (ε > 500 $M^{-1}\cdot cm^{-1}$) indicative of a relatively weak field associated with a five-coordinate metal ion trigonally distorted.[39] In addition, elemental analyses were in good agreement with the proposed stoichiometries for the complexes.

Molecular Structures for 1, 2, 3, and 5. The molecular structures of **1**, **2**, and **5** were determined by X-ray crystallography of single crystals obtained from slow evaporation of distinct 1:1 solvent mixtures. The Oak Ridge thermal ellipsoid plot (ORTEP) diagrams for **2** and **5** are shown in Figure 1 with selected bond lengths and angles comparable to other pentacoordinated systems.[40] The ORTEP of **3** was published previously.[24] Except for the length of the alkyl chains, the perchloro-containing complexes **1**, **2**, and **3** display similar general features including bond lengths and angles, and the ORTEP diagram for **1** is available as Supporting Information (Figure S2). Several attempts to obtain X-ray quality crystals for **4** and **6** were unsuccessful.

The perchloro-complexes **1** and **2** crystallize with an asymmetric unit containing the cationic complex and a perchlorate counterion with no solvent in the lattice. Both complexes display a five-coordinate $[CuN_4O]$ geometry in which the copper ion is bound at the basal plane to, respectively, trans-oriented amine and pyridine nitrogen atoms from each ligand. The Cu−N distances vary from 2.0060(12) to 2.0124(12) Å in **1** and from 2.000(3) to

dx.doi.org/10.1021/ic5004098 | Inorg. Chem. 2014, 53, 5647−5655

2.017(3) Å in **2**. A perchloro coligand completes the coordination sphere through an elongated oxygen bond to the apical position of the metal ion. This longer Cu−O distance reflects a weak apical interaction due to Jahn−Teller distortion in a $3d^9$ ion.[41] The presence of coordinated and uncoordinated ClO_4^- groups is in excellent agreement with the observed IR bands for these species. The bite angles at copper of the amine and pyridine nitrogen atoms from the same ligand are 81.18(5)° and 81.43(5)° for **1** and 81.21(13)° and 81.41(13)° for **2**. The structural parameter $\tau = [(\beta - \alpha)/60]$, with α and β being the two largest angles, is zero for an ideal square pyramid and approaches unity for an ideal trigonal bipyramid.[42] Using this parameter, the calculated τ values for **1** and **2** range from 0.029 to 0.032, thus indicating nearly perfect square pyramidal geometries in the solid state.[43,44] These geometries seem to relax in solution, as inferred from the UV−visible spectrum of these species. The N−Cu−N trans basal angles for **1** are 171.74(5)° and 169.96(5)°, and those of **2** are 171.59(17)° and 169.64(18)°, which are in line with the values expected for a square-pyramidal geometry around Cu(II) complexes.[44] In both structures, a perchlorate counterion forces the structures into a distorted square planar geometry around the copper center, as can be compared to the X-ray structures of the chloride as described below.

Species **5** crystallizes with an asymmetric unit, and the cationic complex also entertains a five-coordinate $[CuN_4X]$ geometry in which the basal plane is defined by the parameters mentioned above but having a *cis*-pyridine and *cis*-amine orientation. Comparable bite angles reach 80.36(6)° and 81.34(6)°, although the trans basal angles of 170.84(7)° and 146.90(5)° deviate significantly from **1** and **2** due to its cis arrangement. The apical site is occupied by a chlorido ligand, which provides less steric hindrance compared to the larger perchlorate ion, thus reflecting a distorted square pyramidal geometry around the copper center with a τ value of 0.40.[38,43] It is noteworthy that from all structurally characterized $[(L^{Py_n})_2Cu^{II}X]X$ species with X = ClO_4^-, NO_3^- Br^-, and Cl^- in this study and elsewhere,[22] this is the first example of cis coordination.

Isothermal Compression and Brewster Angle Microscopy. The behavior of **1**−**6** at the air/water interface was studied by pressure versus area (π vs A) isothermal compression and Brewster angle microscopy (BAM). The compression isotherms were performed to gain information about the behavior of each film at the air/water interface including the general trends for each isotherm, collapse pressure π_c, and nominal collapse area of the monolayer (A_c). During a typical experiment, lateral compression is begun, while the surface tension (γ) of the air/water interface in the presence of the amphiphilic species is measured and compared to the ultrapure air/water interface (γ_0 = 72 mN·m^{-1} at 23 °C), resulting in an increase in π (= $\gamma_0 - \gamma$). BAM is used to study the effects of plane-polarized, reflected laser light as it strikes a medium at the Brewster angle of incidence.[45−47] The technique works on the principle of reflected laser light passing through a minimum while moving between two media of dissimilar refractive indices and has been utilized successfully to study morphologies of numerous two-dimensional films, including domain shapes and homogeneity. After spreading the solution at the air/water interface, a 10 min hold time was used to ensure solvent evaporation prior to lateral compression. Compression isotherms were developed while using BAM to study the film characteristics prior to determining LB deposition pressures. Complex **1** did not provide the amphiphilicity necessary to support successful formation of a film. The possible causes ranged from micelle formation to total dissolution into the subphase. The compression isotherms of **2**−**6** are shown in Figure 2 and discussed below.

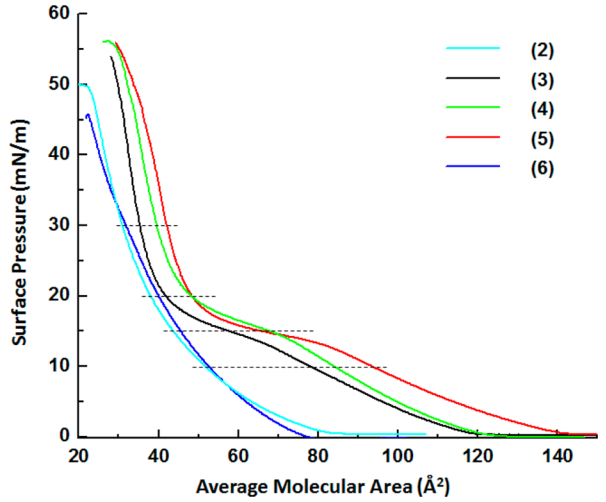

Figure 2. Compression isotherms for **2**−**6**.

After lateral compression, the isothermal behavior of these compounds can be grouped into two general categories: compounds **2** and **6** showed a gradual increase in surface pressure, whereas **3**−**5** display a plateau characteristic of phase transitions. The first group exhibited similar collapse areas per molecule of 42 and 43 Å^2, respectively.

The latter group was composed of systems displaying the L^{PyC18} ligand and collapse π_c at ca. 55 mN·m^{-1}. Average collapse areas per molecule, obtained by extrapolating the steepest part of the curve down to zero pressure,[48] are 44 for **3**, 45 for **4**, and 53 Å^2 for **5**, allowing the establishment of a relationship between the nature of the counterion and the packing order of the film: the bulky perchlorates and nitrates lead to apparently more ordered films than those observed for the chloro-containing species. Those oxoanions, being Hofmeister chaotropes,[49] seem to improve the hydrophilicity of the headgroup fostering greater solubility. Furthermore, when **2** and **6** are analyzed, it seems that a relationship exists between chain length and the nature of the counterion. The presence of bromo ligands in the C_{18}-based **6** suffices to prevent the mesophase transition associated with plateau formation. Similarly, a decrease in the chain length from C_{18} to C_{16}, as in the perchloro-containing **2**—structurally comparable to **3**—also leads to a similar effect.

A comprehensive BAM study of each complex was undertaken to learn about their interfacial behavior and film deposition characteristics. Images and descriptions of the Langmuir films and BAM studies of the ligands L^{Py14}, L^{Py16}, and L^{Py18} are described elsewhere.[22] Comparative BAM images of **2**−**6** at equivalent surface pressures are shown in Figure 3. We begin this discussion with complexes **3**−**5** that exibit a plateau during their isothermal compression. Images of **3** reveal a homogeneous film up to 10 mN·m^{-1} when Newton rings[50] appear, leading to dendritic domain formation at ca. 15−17 mN·m^{-1}. The formation of these domains coincides with the observed plateau during isothermal compression. It has been suggested[51] that anisotropy, as given by the amphiphilic nature

dx.doi.org/10.1021/ic5004098 | Inorg. Chem. 2014, 53, 5647−5655

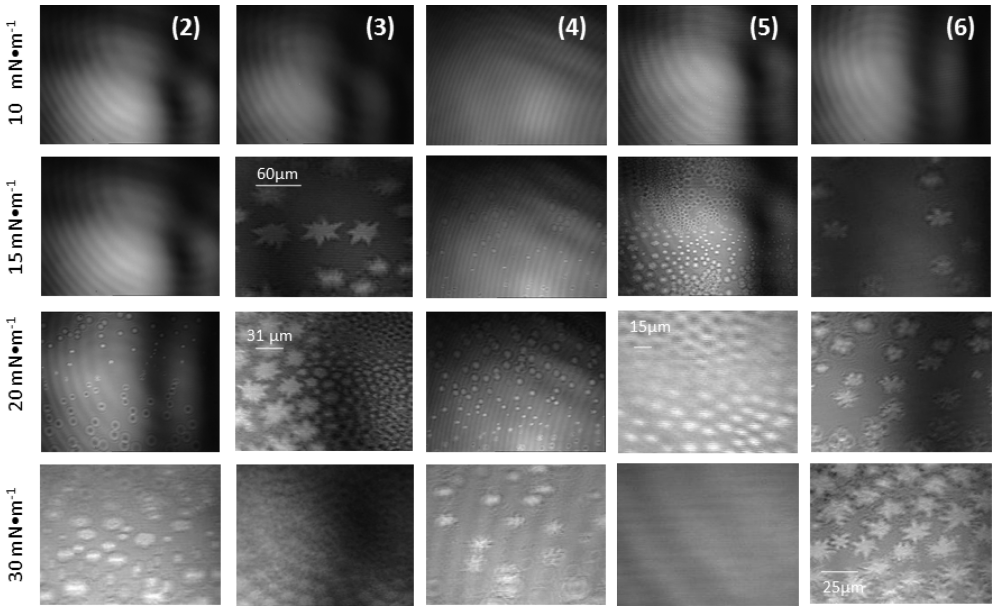

Figure 3. Selected BAM images for species **2**–**6**.

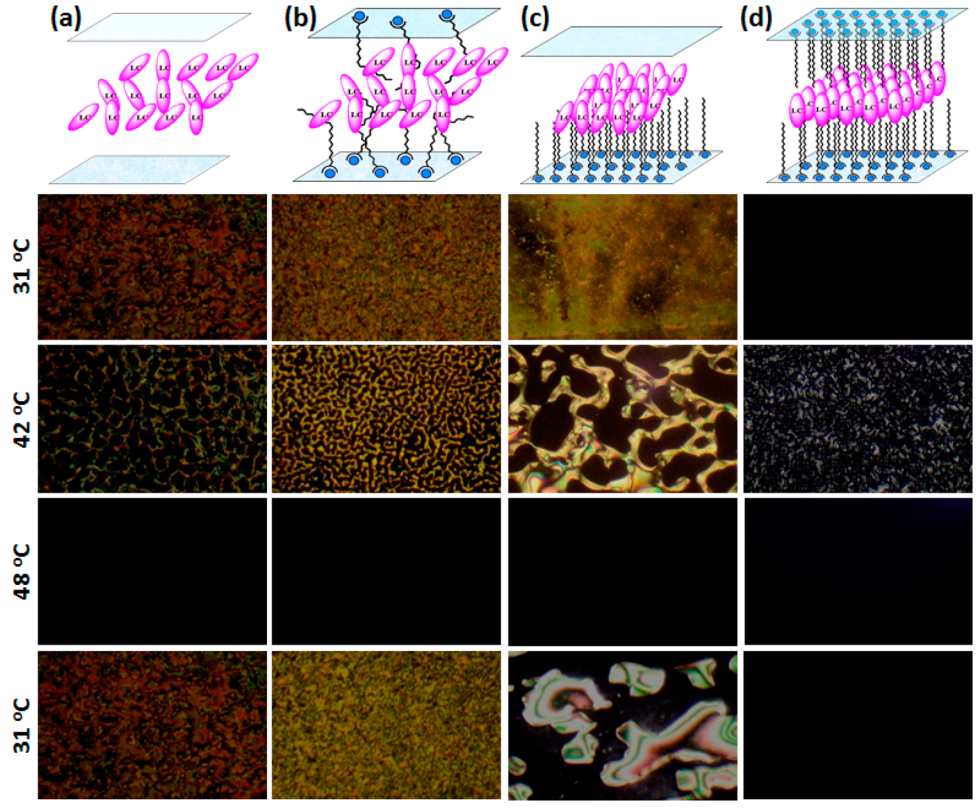

Figure 4. Experimental setups with the organic mesogen MBBA. (a) Control MBBA between untreated slides; (b) MBBA between slides coated with randomly oriented thin film of **3**; (c) MBBA between one uncoated slide and one LB-coated slide; (d) MBBA between two LB-coated slides.

of the complex, provides for the interfacial dynamics required to produce dendritic growth. Disappearance of the dendritic domains coincides with the end of the plateau region of the isotherm, when continued lateral compression encouraged supersaturation on the surface reducing domain sizes from ca. 30 to 5–10 μm up to and through collapse.[52] The BAM images for **4** and **5** bear some resemblance with this pattern in regard to the formation of domains at the plateau surface pressures. However, **4** shows much smaller spherical domains (<5 μm). Dendritic domains, morphologically related to those observed for **3**, only appear at higher surface pressures of ca. 20–30 mN·m^{-1}. These domains multiplied as lateral compression continued, yielding a somewhat homogeneous continuum toward collapse. Interestingly, **5** also leads to a spherical network morphology; however, this happens at lower surface pressures similar to **3**. At higher surface pressures (ca. 25–30 mN·m^{-1}) the film becomes homogeneous, with few apparent defects on the surface up through collapse. In spite of the

dx.doi.org/10.1021/ic5004098 | Inorg. Chem. 2014, 53, 5647–5655

observed homogeneity, this is unlikely to be a monolayer. The driving force for this type of spherical coalescence is the tendency of the molecules to minimize surface energy by reducing interfacial length and curvature.[53]

Species **2** and **6** belong to the group that exhibited gradual increase in surface pressure. On one hand, the former species shows a homogeneous monolayer up to 15 $mN{\cdot}m^{-1}$ when globular domain formation begins and continues increasing in size and number through collapse at 50 $mN{\cdot}m^{-1}$. On the other hand, **6** resembles closely the behavior of **3**; however, the morphological changes seem to take place at consistently higher surface pressures. Hence, noticeable domain formation appears at ca. 20 $mN{\cdot}m^{-1}$. The long C_{18} alkyl chains along with polarizable bromo ligands allow for gradual morphological organization, as observed by the equivalent isotherm. Dendrification has been investigated for other nonmetallated systems, and their growth mechanisms are available.[51,53−57]

Film Deposition of 3 and Its Influence on Liquid Crystalline Ordering. Considering the rugosity of the Langmuir films of **2**−**6**, we hypothesize that such morphologies can affect the alignment of liquid crystals deposited at the surface of these LB films. Although the influence of thin films on the orientation of liquid crystals has been established,[58,59] the topic has received renewed interest due to experimental and theoretical advancements;[25,27] reports describe modified mesogen behavior in the presence of organic self-assembled monolayers containing polyelectrolytes,[28] cyanobiphenyl,[29] sulfonate surfactants,[30] alkanethiols,[31] and even sodium salts with different anions.[26] To the best of our knowledge, neither metallosurfactants nor LB films have been studied. Therefore, we selected **3**, deposited at 18 $mN{\cdot}m^{-1}$, to be used in preliminary studies assessing the use of metallosurfactant-based LB films as inducers of liquid crystalline alignment. This surface pressure coincides with the end of the plateau observed during isothermal compression, which relates to a rugged morphology. We used MBBA, a common liquid crystalline material that exhibits nematic behavior. The molecules in a nematic phase adopt some degree of averaged orientational order with respect to a director, along with limited translational order characterized by the absence of layer formation. The optical properties resulting from molecular orientation can be controlled by the application of electric fields, thus making them relevant to information display, which is commonly used in LCD technology.

Four experimental setups were developed where a sample of MBBA was sandwiched between glass slides under different conditions: (a) a control setup where the mesogen is sandwiched between untreated slides; (b) another control where the mesogen is placed between two slides coated with a randomly oriented thin film of **3** resulting from solvent evaporation; (c) a setup where the mesogen MBBA is placed between an uncoated slide and a glass slide coated with a single monolayer of species **3** deposited at 18 $mN{\cdot}m^{-1}$; (d) a setup where MBBA is sandwiched between two slides coated with an LB monolayer. Each setup was inserted into the microscope, heated above the isotropic temperature of MBBA, and then allowed to cool to room temperature. Figure 4 shows the schematic setups for (a) through (d) along with the equivalent behavior observed for the mesogen MBBA.

The nematic liquid crystal MBBA has two different indices of refraction, 1.75 and 1.54 at 25 °C.[60] Because of its birefringent nature, when linearly polarized light is directed at a certain angle with respect to the optical axis, parallel and perpendicular components travel different optical path lengths over the same physical distance. This leads to elliptically polarized light. When MBBA is heated into its isotropic state, crossed polarizers will not allow light to pass and will appear black. However, since room temperature MBBA alters the orientation of linearly polarized light to elliptically polarized light, when it is placed between perpendicularly oriented polarizers some residual light is transmitted. This allows the nematic and isotropic states of MBBA to be easily distinguished. The control setup (a) exhibits the expected phase changes associated with heating MBBA. A nematic phase is observed at 31 °C and moves to the isotropic phase at 42 °C. At 48 °C it is completely isotropic. The original phase is restored upon cooling to 31 °C. In the control setup (b) species **3** was dripped onto each slide using a pipet. After the solvent chloroform was evaporated, one drop of the liquid crystal was deposited. In this case, the resulting film pattern on the slide is expected to lack orientational order, thus playing a minor role on the alignment of the liquid crystal. Indeed, only negligible changes are observed. Cooling back to 31 °C yields a texture that is closely related to the original one. The similarity between the experimental setups (a) and (b) is expected because in the latter experiment MBBA was deposited to a slide with a randomly ordered film. Considerable changes, however, are observed for setups (c) and especially (d), involving the use of glass slides coated with LB films of **3** deposited at 18 $mN{\cdot}m^{-1}$. For setup (c) the deposited LB monolayer of **3** on the slide begins to influence the organizational nature of the liquid crystal. This is only slightly apparent when the cell is first put together and the sample is viewed in its nematic phase at 31 °C. When, however, the sample is heated up well into the isotropic phase at 48 °C and then cooled back into the nematic at 31 °C, the resulting texture is significantly different from what it was before at this same temperature. Many regions of the nematic now appear dark because the molecules are aligned perpendicularly to the glass surface in what is called the homeotropic or pseudoisotropic texture where the optic axis is parallel to the viewing direction. But this alignment is not complete as may be deduced from the existence of regions that are not dark. With setup (d), where *two* coated slides impose homeotropic alignment, the liquid crystal immediately adopts the homeotropic alignment at room temperature. There is some minor loss of this alignment near the phase transition at 42 °C as may be seen in the figure, but then the sample again turns dark as it is heated into the isotropic phase. Upon cooling it reverses back through the same stages, finally adopting the dark homeotropic texture seen at 31 °C.

■ SUMMARY AND CONCLUSIONS

In this Article we discussed the synthesis of new pyridine-based amphiphilic ligands displaying decyl-, hexadecyl-, and octadecylamine alkyl chains. Treatment of these ligands with copper(II) salts yielded new double-tail cationic copper(II)-containing surfactants **1**−**5** that were isolated as crystalline (**1**, **2**, **5**) or microcrystalline (**3**, **4**, **6**) species and were characterized by ESI^+ mass spectrometry, IR spectroscopy, elemental analyses, and melting points. A five-coordinate $[CuN_4X]$ geometry describes the coordination around the copper ion, bound at the basal plane to the amine and pyridine nitrogen atoms of the ligands L^{PY_n} and to a negatively charged apical coligand. The isothermal compression of these compounds has shown that the hydrophobic chains must be at least 16 carbons long to yield the necessary amphiphilicity required for efficient LB film formation, leading to a detailed study of species **2**−**6**. These

dx.doi.org/10.1021/ic5004098 | Inorg. Chem. 2014, 53, 5647−5655

species could then be sorted into two groups, one displaying a gradual increase in surface pressure (**2** and **6**) and another showing a plateau-marked phase transition (**3**–**5**). Brewster angle microscopy revealed an eventful interfacial chemistry marked by morphological changes associated with surface pressure increase. The Langmuir films display domains of variable globular to dendritic morphology. At higher pressures a homogeneous multilayer seems to be formed. Langmuir films of the metallosurfactant **3** were deposited and studied as potential directors for liquid crystalline alignment; while randomly oriented films of **3** do not affect the mesogen MBBA, the presence of LB-coated films on the surfaces leads to pronounced alignment.

These findings serve as a stepping stone toward the development of responsive materials based on redox-active metallosurfactants. Future studies will focus on understanding how the electrochemical reduction of these metallosurfactants might induce geometrical changes in the Langmuir films, thus changing the interactions between the films and the mesogenic material.

■ ASSOCIATED CONTENT

Ⓢ Supporting Information

Mass spectrometric patterns for the cationic species $[(L^{Py18})_2Cu^{II}NO_3]^+$ and $[(L^{Py18})_2Cu^{II}Br]^+$ and the ORTEP diagram for the cation $[(L^{Py14})_2Cu^{II}ClO_4]^+$. This material is available free of charge via the Internet at http://pubs.acs.org. The crystal structures for compounds **1**, **2**, and **5** were deposited at the Cambridge Crystallographic Data Centre and allocated the respective deposition numbers of 933201, 933202, and 933203.

■ AUTHOR INFORMATION

Corresponding Author

*E-mail: cnverani@chem.wayne.edu. Phone: 313 577 1076.

Notes

The authors declare no competing financial interest.

■ ACKNOWLEDGMENTS

C.N.V. gratefully thanks the National Science Foundation (Grant CHE-1012413) for financial support.

■ REFERENCES

(1) Gohy, J. F.; Lohmeijer, B. G. G.; Schubert, U. S. *Chem.—Eur. J.* **2003**, *9*, 3472–3479.
(2) Gaspar, A. B.; Seredyuk, M.; Gutlich, P. *Coord. Chem. Rev.* **2009**, *253*, 2399–2413.
(3) Binnemans, K.; Görller-Walrand, C. *Chem. Rev.* **2002**, *102*, 2303–2346.
(4) Joy, S.; Pal, P.; Mondal, T. K.; Talapatra, G. B.; Goswami, S. *Chem.—Eur. J.* **2012**, *18*, 1761–1771.
(5) Bolink, H. J.; Baranoff, E.; Clemente-Leon, M.; Coronado, E.; Lardies, N.; Lopez-Munoz, A.; Repetto, D.; Nazeeruddin, Md. K. *Langmuir* **2010**, *26*, 11461–11468.
(6) Park, J.; Pasupathy, A. N.; Goldsmith, J. I.; Chang, C.; Yaish, Y.; Petta, J. R.; Rinkoski, M.; Sethna, J. P.; Abruna, H. D.; McEuen, P. L.; Ralph, D. C. *Nature* **2002**, *417*, 722–725.
(7) (a) Whittell, G. R.; Hager, M. D.; Schubert, U. S.; Manners, I. *Nat. Mater.* **2011**, *10*, 176–188. (b) Wassel, R. A.; Gorman, C. B. *Angew. Chem., Int. Ed.* **2004**, *43*, 5120–5123.
(8) Wickramasinghe, L. D.; Perera, M. M.; Li, L.; Mao, G.; Zhou, Z.; Verani, C. N. *Angew. Chem., Int. Ed.* **2013**, *52*, 13346–13350.
(9) Carlton, R. J.; Hunter, J. T.; Miller, D. S.; Abbasi, R.; Mushenheim, P. C.; Tan, L. N.; Abbott, N. L. *Liq. Cryst. Rev.* **2013**, 2–23.
(10) Kraus, S.; Mandler, D. *Langmuir* **2006**, *22*, 7462–7464.
(11) Chico, R.; Domínguez, C.; Donnio, B.; Coco, S.; Espinet, P. *Dalton Trans.* **2011**, *40*, 5977–5983.
(12) Guerrero-Martinez, A.; Vida, Y.; Dominguez-Gutierrez, D.; Albuquerque, R. Q.; de Cola, L. *Inorg. Chem.* **2008**, *47*, 9131–9133.
(13) Muñoz, M. J. M.; Fernández, G. *Chem. Sci.* **2012**, *3*, 1395–1398.
(14) Kobayashi, K.; Tonegawa, N.; Fujii, S.; Hikida, J.; Nozoye, H.; Tsutsui, K.; Wada, Y.; Chikira, M.; Haga, M.-A. *Langmuir* **2008**, *24*, 13203–13211.
(15) Shakya, R.; Allard, M. M.; Johann, M.; Heeg, M. J.; Rentschler, E.; Shearer, J. M.; McGarvey, B. R.; Verani, C. N. *Inorg. Chem.* **2011**, *50*, 8356–8366.
(16) Lesh, F. D.; Shanmugam, R.; Allard, M. M.; Lanznaster, M.; Heeg, M. J.; Rodgers, M. T.; Shearer, J. M.; Verani, C. N. *Inorg. Chem.* **2010**, *49*, 7226–7228.
(17) Lesh, F. D.; Hindo, S. S.; Allard, M. M.; Jain, P.; Peng, B.; Hryhorczuk, L.; Verani, C. N. *Eur. J. Inorg. Chem.* **2009**, *3*, 345–356.
(18) Shakya, R.; Hindo, S. S.; Wu, L.; Allard, M. M.; Heeg, M. J.; Hratchian, H. P.; McGarvey, B. R.; da Rocha, S. R. P.; Verani, C. N. *Inorg. Chem.* **2007**, *46*, 9808–9818.
(19) Hindo, S. S.; Shakya, R.; Rannulu, N. S.; Allard, M. M.; Heeg, M. J.; Rodgers, M. T.; da Rocha, S. R.; Verani, C. N. *Inorg. Chem.* **2008**, *47*, 3119–3127.
(20) Shakya, R.; Hindo, S. S.; Wu, L.; Ni, S.; Allard, M. M.; Heeg, M. J.; da Rocha, S. R. P.; Yee, G. T.; Hratchian, H. P.; Verani, C. N. *Chem.—Eur. J.* **2007**, *13*, 9948–9956.
(21) Hindo, S. S.; Shakya, R.; Shanmugam, R.; Heeg, M. J.; Verani, C. N. *Eur. J. Inorg. Chem.* **2009**, *31*, 4686–4694.
(22) Driscoll, J. A.; Allard, M. M.; Wu, L.; Heeg, M. J.; da Rocha, S. R. P.; Verani, C. N. *Chem.—Eur. J.* **2008**, *14*, 9665–9674.
(23) Jayathilake, H. D.; Driscoll, J. A.; Bordenyuk, A. N.; Wu, L.; da Rocha, S. R. P.; Verani, C. N.; Benderskii, A. V. *Langmuir* **2009**, *25*, 6880–6886.
(24) Driscoll, J. A.; Keyes, P. H.; Heeg, M. J.; Heiney, P. A.; Verani, C. N. *Inorg. Chem.* **2008**, *47*, 7225–7232.
(25) Miller, D. S.; Carlton, R. J.; Mushenheim, P. C.; Abbott, N. L. *Langmuir* **2013**, *29*, 3154–3169.
(26) Carlton, R. J.; Ma, C. D.; Gupta, J. K.; Abbott, N. L. *Langmuir* **2012**, *28*, 12796–12805.
(27) Lowe, A. M.; Ozer, B. H.; Bai, Y.; Bertics, P. J.; Abbott, N. L. *ACS Appl. Mater. Interfaces* **2010**, *2*, 722–731.
(28) Zou, J.; Fang, J. *Langmuir* **2010**, *26*, 7025–7028.
(29) Prompinit, P.; Achalkumar, A. S.; Bramble, J. P.; Bushby, R. J.; Wälti, C.; Evans, S. D. *ACS Appl. Mater. Interface* **2010**, *2*, 3686–3692.
(30) Lockwood, N. A.; de Pablo, J. J.; Abbott, N. L. *Langmuir* **2005**, *21*, 6805–6814.
(31) Brake, J. M.; Abbott, N. L. *Langmuir* **2002**, *18*, 6101–6109.
(32) Theoretical: Greschek, M.; Gubbins, K. E.; Schoen, M. *J. Chem. Phys.* **2012**, *137*, 144703–1–144703–10.
(33) Pikina, E.; Rosenblatt, C. *Eur. Phys. J. E* **2012**, *35*, 87–1–87–19.
(34) *APEX II, SMART, SAINT and SADABS* collection and processing programs are distributed by the manufacturer; Bruker AXS, Inc.: Madison WI, 2004.
(35) Sheldrick, G., *SHELX-97;* University of Gottingen: Gottingen, Germany, 1997.
(36) Gopal, A.; Belyi, V. A.; Diamant, H.; Witten, T. A.; Lee, K. Y. C. *J. Phys. Chem. B* **2006**, *110*, 10220–10223.
(37) Nakamoto, K. Chapter 1. In *Infrared and Raman Spectra of Inorganic and Coordination Compounds, Part B: Applications in Coordination, Organometallic and Bioinorganic Chemistry,* 6th ed.; John Wiley & Sons, Inc.: Hoboken, NJ, 2008; pp 1–222.
(38) Valencia, L.; Bastida, R.; F.-Fernandez, M. C.; Macias, A.; Vicente, M. *Inorg. Chim. Acta* **2005**, *358*, 2618–2628.
(39) Lever, A. B. P. *Inorganic Electronic Spectroscopy,* 2nd ed.; Elsevier Science: Amsterdam, 1984; p 689.

(40) Blake, A. J.; Danks, J. P.; Li, W. S.; Lippolis, V.; Schröder, M. *J. Chem. Soc., Dalton Trans.* **2000**, 3034−3040.
(41) Mukherjee, A.; Nethaji, M.; Chakravarty, A. R. *Polyhedron* **2004**, *23*, 3081−3085.
(42) Addison, A. W.; Rao, T. N.; Reedijk, J.; van Rijn, J.; Verschoor, G. C. *J. Chem. Soc., Dalton Trans.* **1984**, 1349−1356.
(43) Hegg, E. L.; Mortimore, S. H.; Cheung, C. L.; Huyett, J. E.; Powell, D. R.; Burstyn, J. N. *Inorg. Chem.* **1999**, *38*, 2961−2968.
(44) Holmes, R. R. *J. Am. Chem. Soc.* **1984**, *106*, 3745−3750.
(45) Honig, D.; Möbius, D. *J. Phys. Chem.* **1991**, *95*, 4590−4592.
(46) Henon, S.; Meunier, J. *Rev. Sci. Instrum.* **1991**, *62*, 936−939.
(47) Gericke, A.; Michailov, A. V.; Huhnerfuss, H. *Vib. Spectrosc.* **1993**, *4*, 335−348.
(48) Talham, D. R. *Chem. Rev.* **2004**, *104*, 5479−5501.
(49) Cho, Y.; Zhang, Y.; Christensen, T.; Sagle, L. B.; Chilkoti, A.; Cremer, P. S. *J. Phys. Chem. B* **2008**, *112*, 13765−13771.
(50) G.-Miyoshi, J.; Ramos, S.; R.-Garcia, J.; Castillo, R. *J. Chem. Phys.* **2001**, *115*, 8178−8184.
(51) Iimura, K.; Yamauchi, Y.; Tsuchiya, Y.; Kato, T.; Suzuki, M. *Langmuir* **2001**, *17*, 4602−4609.
(52) Gutierrez-Campos, A.; Diaz-Leines, G.; Castillo, R. *J. Phys. Chem. B* **2010**, *114*, 5034−5046.
(53) Knobler, C. M. *Science* **1990**, *249*, 870−874.
(54) Couder, Y.; Maurer, J.; González-Cinca, R.; Hernández-Machado, A. *Phys. Rev. E: Stat., Nonlinear, Soft Matter Phys.* **2005**, *71*, 031602−1−031602−12.
(55) Melzer, V.; Vollhardt, D.; Brezesinski, G.; Mohwald, H. *J. Phys. Chem. B* **1998**, *102*, 591−597.
(56) Doughtery, A.; Kaplan, P. D.; Gollub, J. P. *Phys. Rev. Lett.* **1987**, *58*, 1652−1655.
(57) Honda, T.; Honjo, H.; Katsuragi, H. *J. Cryst. Growth* **2005**, *275*, e225−e228.
(58) Cognard, J. *Mol. Cryst. Liq. Cryst.* **1981**, *64*, 331−342.
(59) Janning, J. L. *Appl. Phys. Lett.* **1972**, *21*, 173−174.
(60) Kowel, S.; Kornreich, P.; Cleverly, D. *Appl. Opt.* **1984**, *23*, 278−289.